Studies in Surf. Sci. & Catal., **2000**, v.129, p. 597-606.

Calculations of Pore Size Distributions in Nanoporous Materials from Adsorption and Desorption Isotherms

Peter I. Ravikovitch and Alexander V. Neimark

TRI/Princeton, 601 Prospect Av., Princeton, NJ, 08542-0625, ravikovi@triprinceton.org, aneimark@triprinceton.org

The recently developed density functional theory method for pore size distribution analysis from nitrogen adsorption and desorption isotherms is extended to materials with pores ranging from 2 to 100 nm. The method is based on the nonlocal density functional theory (NLDFT) of capillary condensation hysteresis in cylindrical pores. It is shown that NLDFT correctly predicts both the adsorption and desorption branches of the hysteretic isotherms in materials with cylindrical pores wider than ca. 5 nm. For pores larger than ca. 6 nm, the NLDFT results agree well with the thermodynamic theory of Derjaguin-Broekhoff-de Boer. When pore-blocking (networking) effects are insignificant, both branches of the experimental isotherm produce identical pore size distributions. The NLDFT method is validated against literature data on capillary condensation in MCM-41 type materials with pores from 5 to10 nm.

1. INTRODUCTION

After the breakthrough discovery of mesoporous molecular sieves of M41S type [1] new periodically structured materials have been synthesized with pores covering the whole mesoporous domain of 2-20 nm. Enlarged MCM-41 materials [2-4] and other well-ordered mesoporous structures [5-7] with pores wider than 4-5 nm are of special interest for the theory of capillary phenomena. Unlike standard MCM-41 and MCM-48 samples, which typically contain pores of 3-4 nm, low temperature nitrogen adsorption-desorption isotherms on larger pore materials form a well-defined hysteresis loop, whose origin has been the focus of intense studies and discussions for more than fifty years [8-20]. From the practical viewpoint of pore structure characterization, the adsorption-desorption hysteresis presents a problem of choice of a suitable branch of the isotherm for the pore size distribution calculations [14]. The results obtained from different branches of the isotherm are usually significantly different.

According to the classical treatment of Cohan [8], which is the basis of the conventional BJH method [14], capillary condensation in an infinite cylindrical pore is described by the Kelvin equation using cylindrical meniscus, while desorption is associated with spherical meniscus. In large pores the following asymptotic equation is expected to be valid [8]: $P_D/P_0 = (P_A/P_0)^2$, where P_D/P_0 and P_A/P_0 are the relative pressures of the desorption and adsorption, respectively. An improved treatment [9-

11, 13], originated from Derjaguin [9], takes into account the influence of surface forces on adsorbed film equilibrium and stability, which leads to predictions for capillary condensation and desorption pressures, substantially different from those of Cohan's theory, even in relatively large pores.

Recent progress in understanding capillary condensation deals with molecular level models. The methods of the grand canonical Monte Carlo (GCMC) simulations [17], molecular dynamics (MD) [18], and density functional theory (DFT) [19] allow direct modeling of capillary condensation/desorption phase transitions, and are capable of generating hysteresis loops of simple fluids sorbed in model pores. In our previous publications [20-24], we have shown that the non-local density functional theory (NLDFT) with properly chosen parameters of fluid-fluid and fluid-solid intermolecular interactions quantitatively predicts desorption branches of hysteretic isotherms of nitrogen and argon on reference MCM-41 samples with pore channels narrower than 5 nm. A new method for calculating pore size distributions from the desorption branch of the isotherm has been developed and tested against reference experiments on high-quality MCM-41 materials [23] and direct Monte Carlo simulations [17]. The NLDFT method gives reliable estimates of pore sizes and pore wall thicknesses in MCM-41 materials [23] and catalysts [21, 22, 24].

In this paper, we extend the NLDFT method to larger pore MCM-41 materials, whose nitrogen isotherms exhibit prominent hysteresis. Density functional theory is especially suitable for modeling adsorption isotherms in large pores, and is likely the most feasible technique for testing the reliability of conventional macroscopic approaches. We demonstrate that the NLDFT model provides accurate agreement between calculations and experiments for both adsorption and desorption branches of nitrogen isotherms on newly synthesized enlarged MCM-41 type materials with pore channels in the range from 5 to 10 nm [2-4]. We conclude that in the range of pore sizes > ca. 5 nm, the experimental desorption branch corresponds to the equilibrium evaporation, while the experimental capillary condensation branch corresponds to the spontaneous (spinodal) condensation. Moreover, the NLDFT predictions of equilibrium and spontaneous capillary condensation transitions for pores wider than 6 nm are well approximated by the macroscopic equations of the Derjaguin-Broekhoff-de Boer theory [10,11], while the results of the traditional Cohan equations (the BJH method) are significantly in error.

Two kernels of theoretical isotherms in cylindrical channels have been constructed corresponding to the adsorption and desorption branches. For a series of samples [2-4], we show that the pore size distributions calculated from the experimental desorption branches by means of the desorption kernel satisfactory coincide with those calculated from the experimental adsorption branches by means of the adsorption kernel. This provides a convincing argument in favor of using the NLDFT model for pore size characterization of nanoporous materials provided that the adsorption and desorption data are processed consistently.

2. NONLOCAL DENSITY FUNCTIONAL THEORY OF ADSORPTION HYSTERESIS

In the density functional theory, the structure and thermodynamics of confined fluids are predicted from the intermolecular potentials of the fluid-fluid and solid-fluid interactions. To model nitrogen adsorption, we employ a version of the NLDFT based on the Tarazona's smoothed density

approximation [19]. A detailed description of the theory has been given in our previous publications (see e.g. [23] and references therein).

Predictions of the density functional theory depend largely on the correct choice of the parameters of intermolecular interactions. Parameters of the Lennard-Jones potential describing the fluid-fluid interactions have been optimized to provide an accurate description of the two-phase equilibrium in bulk nitrogen, including the surface tension of the liquid-gas interface [23]. Interactions between solid and fluid are approximated using the potential in an infinite cylindrical pore [25]. Parameters of solid-fluid interactions have been chosen to provide the best possible fit to the standard nitrogen isotherm on nonporous oxides [26]. A comparison of the calculated excess adsorption isotherm in a large cylindrical pore of 107 nm with the standard nitrogen isotherm is presented in Figure 1a. The steps on the calculated isotherm are caused by the structureless pore wall model used. On average however, the calculated adsorption isotherm agrees well with the experimental data as it is seen from the corresponding t-plot (Figure 1b).

The adsorption and desorption isotherms have been calculated for the N_2 sorption at 77K in cylindrical pores in the range 2-100 nm. The points of equilibrium and spinodal transitions are plotted in Fig. 2 in comparison with the adsorption and desorption points calculated according to standard Cohan's equations using the same nitrogen standard isotherm [26]. There are several features worth noting. The line of equilibrium capillary condensation asymptotically approaches the Kelvin equation for the spherical meniscus and the line of spontaneous capillary condensation asymptotically approaches the Kelvin equation for the cylindrical meniscus. This asymptotic behavior is in agreement with the classical scenario of capillary hysteresis [12]: capillary condensation occurs spontaneously after the formation of the cylindrical adsorption film on the pore walls while evaporation occurs after the formation of the equilibrium meniscus at the pore end. As the pore size decreases, the surface forces come forefront and deviations from the classical picture become significant even for pores as large as 10-20 nm.

Much better agreement has been found with the results of the Derjaguin-Broekhoff-de Boer theory [10,11] (Figure 3, top). For pores wider than ca. 6 nm the equilibrium and spontaneous capillary condensation transitions predicted by the NLDFT are well approximated by the semi-empirical equations of Broekhoff and de Boer [10,11]. In smaller pores, the deviations are substantial (Figure 3, bottom).

The NLDFT predicts the critical point for capillary condensation phase transition (capillary critical pore size) at ca. 2 nm, which is approximately the minimum pore size in which capillary condensation is experimentally observed [21,27]. However, the theory fails to predict the disappearance of the hysteresis loop for pores smaller than ca. 4 nm (hysteresis critical point) [20,15]. It should be noted that the theory of Broekhoff and de Boer fails to predict both critical points unless some additional semi-empirical corrections are made [16].

Recent Monte Carlo simulations of N_2 in cylindrical pores fully support the results of the NLDFT calculations [28]. Thus, it appears that the failure of the NLDFT to predict the disappearance of the hysteresis loop at relative pressures below ca. 0.4 and pores smaller than ca. 4 nm is of a fundamental nature and cannot be explained by approximations made in the theory.

Studies in Surf. Sci. & Catal., **2000**, v.129, p. 597-606.

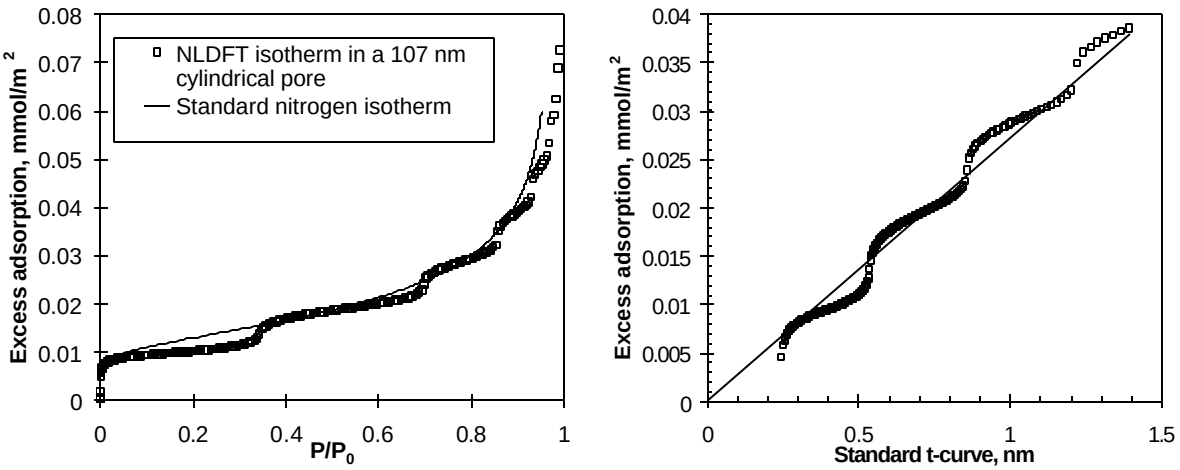

Figure 1. (a) Comparison of the NLDFT isotherm in a 107 nm diameter cylindrical pore with the standard nitrogen isotherm on nonporous oxides [26]. (b) corresponding statistical film thickness plot.

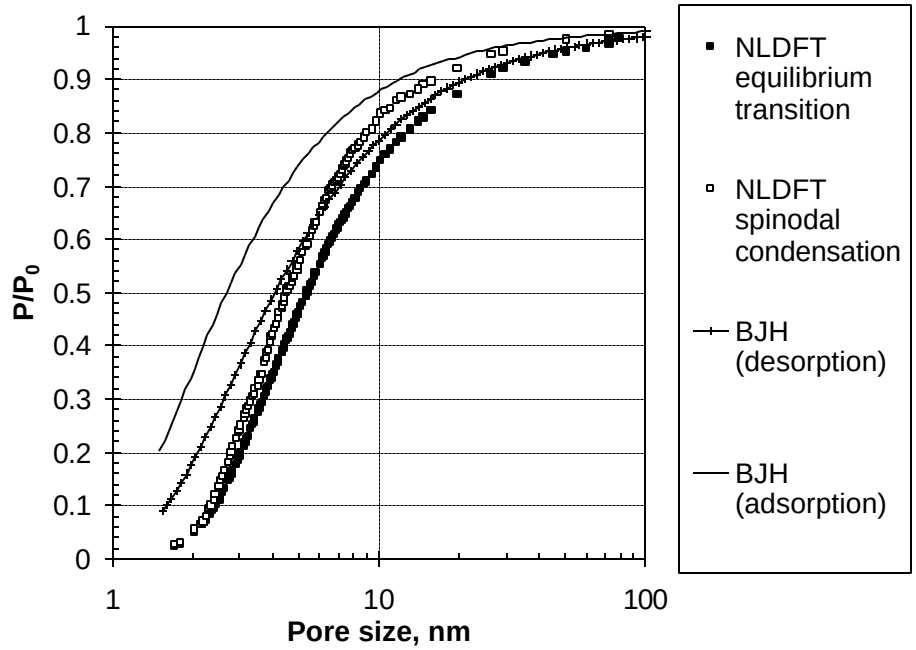

Figure 2. Capillary hysteresis of nitrogen in cylindrical pores at 77 K. Equilibrium desorption (black squares) and spinodal condensation (open squares) pressures predicted by the NLDFT in comparison with the results of Cohan's equation (the BJH method) for spherical (crosses and line) and cylindrical (line) meniscus.

Studies in Surf. Sci. & Catal., **2000**, v.129, p. 597-606.

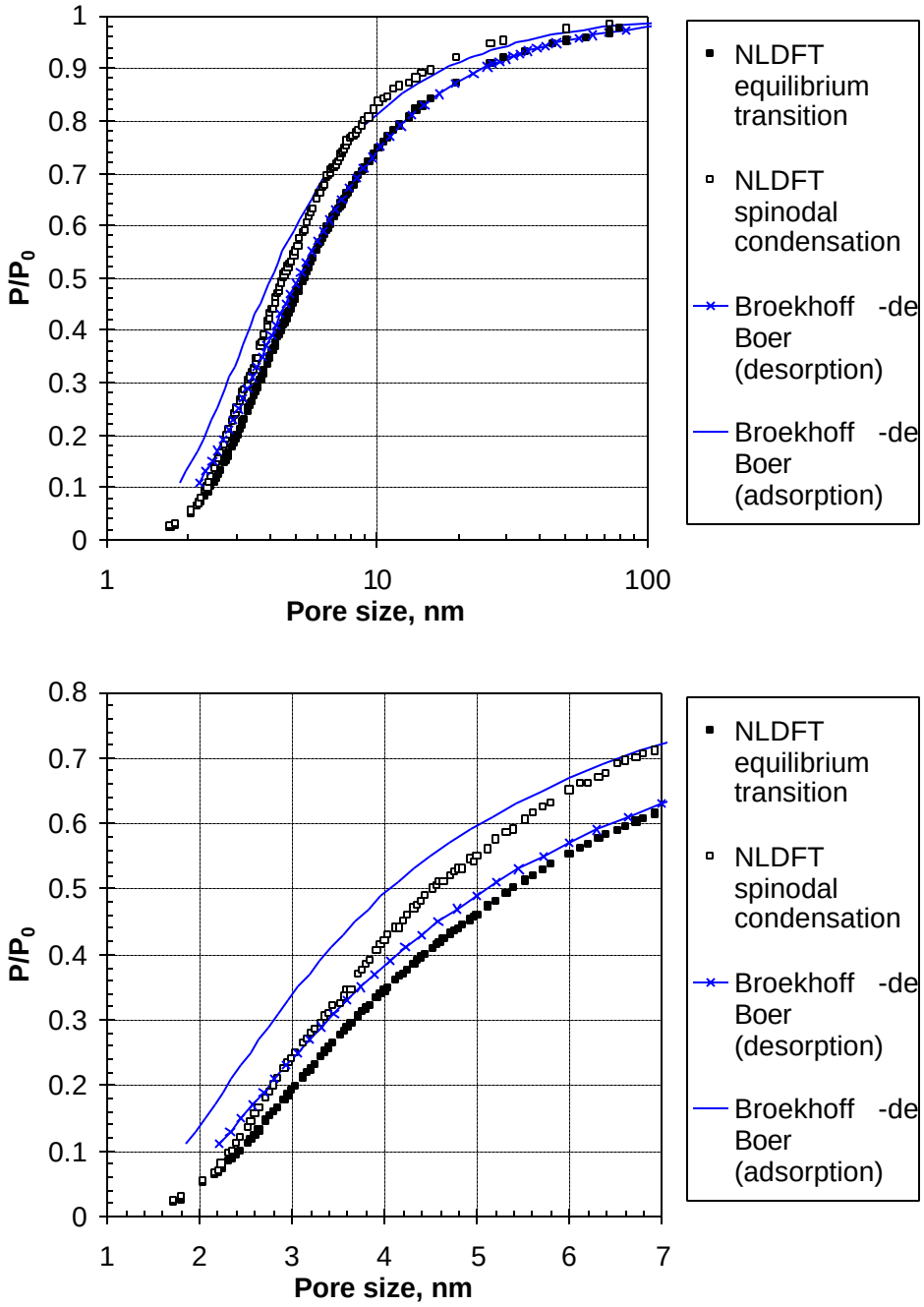

Figure 3. Capillary hysteresis of nitrogen in cylindrical pores at 77 K. Equilibrium desorption (black squares) and spontaneous condensation (open squares) pressures predicted by the NLDFT in comparison with the results of the Broekhoff and de Boer theory [10, 11].

3. COMPARISON WITH EXPERIMENTS AND CALCULATION OF PORE SIZE DISTRIBUTIONS

From our earlier studies, we have made the following general conclusions regarding capillary condensation in cylindrical pores [20, 22, 23]. Reversible isotherms in sufficiently narrow pores and desorption branches of the hysteretic isotherms in wider pores correspond to the equilibrium transitions predicted by the NLDFT. The adsorption branches of hysteretic isotherms lie inside the theoretical hysteresis loop. These conclusions were made based on analyses of limited experimental data on reference MCM-41 materials with pores < 5nm. Sayari et al. [2-4] have recently synthesized enlarged MCM-41-type samples with pore diameters from 5 to 10 nm. The N_2 isotherms on two of these samples are presented in Figs. 4-5 in comparison with the theoretical hysteresis loops for cylindrical pores of an average size, formed by the metastable adsorption branch and the equilibrium desorption branch. The experimental and theoretical hysteresis loops are in good qualitative agreement.

To calculate the pore size distributions we have constructed two kernels of theoretical isotherms in cylindrical channels corresponding to the metastable adsorption and equilibrium desorption branches. These kernels were employed for calculating pore size distributions from experimental isotherms following the deconvolution procedure described elsewhere [21, 24]. In Figs. 6-7 we present the pore size distributions of the enlarged MCM-41 samples [2-4] calculated from the experimental desorption branches by means of the desorption kernel and the pore size distributions calculated from the experimental adsorption branches by means of the adsorption kernel. The pore size distributions obtained from the desorption and adsorption branches practically coincide, which confirms that the NLDFT quantitatively describes both branches on the adsorption-desorption isotherm.

Structural parameters of the MCM-41 materials calculated by means of the NLDFT method are listed in Table 1. We note very good agreement between the results obtained from the desorption and adsorption branches of the isotherms, especially for samples #1 - #3. It is worth noting that the pore wall thickness (1.2-1.8 nm) of wide-pore MCM-41 materials is larger than that usually obtained for conventional MCM-41, and tends to increase with the pore diameter.

4. CONCLUSIONS

The non-local density functional theory (NLDFT) with properly chosen parameters of fluid-fluid and fluid-solid intermolecular interactions quantitatively predicts both adsorption and desorption branches of capillary condensation isotherms on MCM-41 materials with pore sizes from 5 to 10 nm. When pore-blocking (networking) effects are insignificant, the pore size distributions calculated from the adsorption and desorption branches of the experimental isotherm are in good agreement. For materials with a wide hysteresis loop of IUPAC's type H2 [14], which is usually attributed to pore blocking [29,30], the use of the adsorption branch may yield more reliable results, provided the kernel of metastable adsorption isotherms is employed. For samples with smaller pores (< 5 nm), the equilibrium desorption branch has the advantage of being theoretically more accurate. In this case we recommend using desorption isotherms for estimating pore size distributions in mesoporous materials of the MCM-41 type.

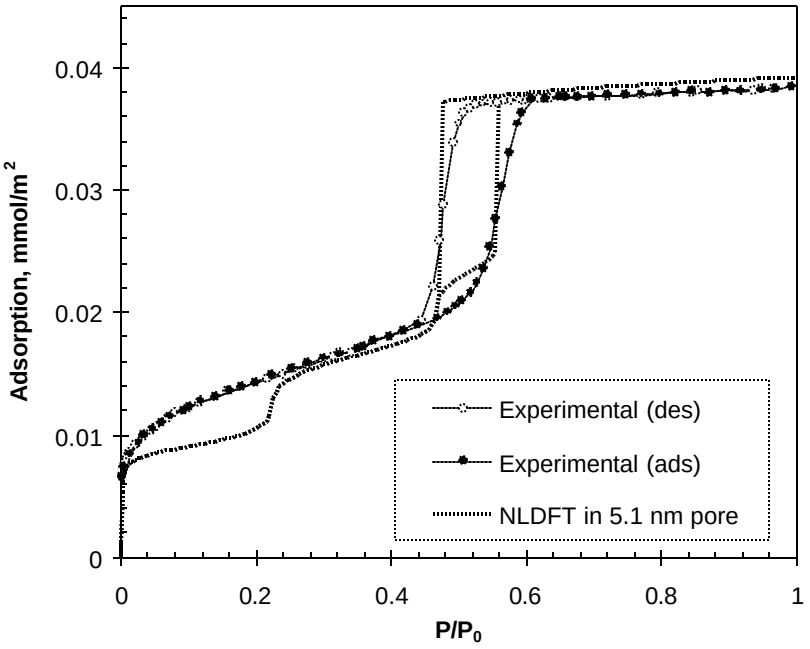

Figure 4. Comparison of the NLDFT N_2 isotherm in 5.1 nm cylindrical pore at 77 K with the isotherm on enlarged MCM-41 material [2, 3] (sample #1 in Table 1).

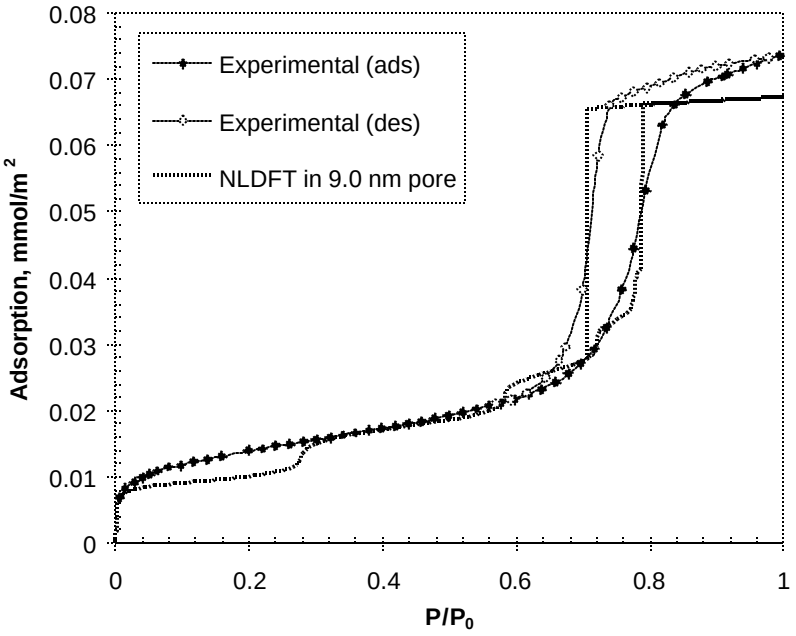

Figure 5. Comparison of the NLDFT N_2 isotherm in 9 nm cylindrical pore at 77 K with the isotherm on a wide-pore material [4] (sample #4 in Table 1).

Studies in Surf. Sci. & Catal., **2000**, v.129, p. 597-606.

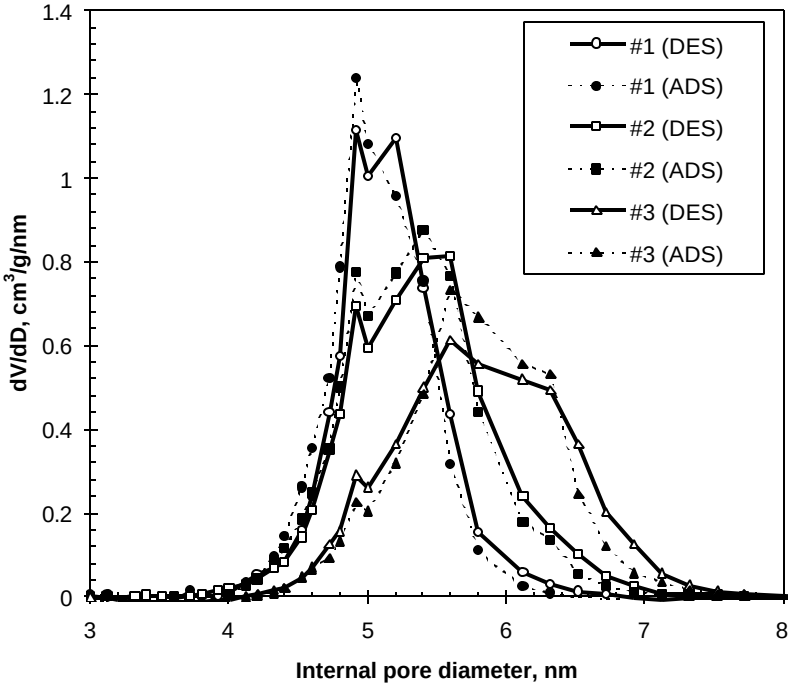

Figure 6. The pore size distributions of enlarged MCM-41 materials [2-3] calculated from adsorption (dotted lines) and desorption (solid lines) branches of nitrogen isotherms by the NLDFT method.

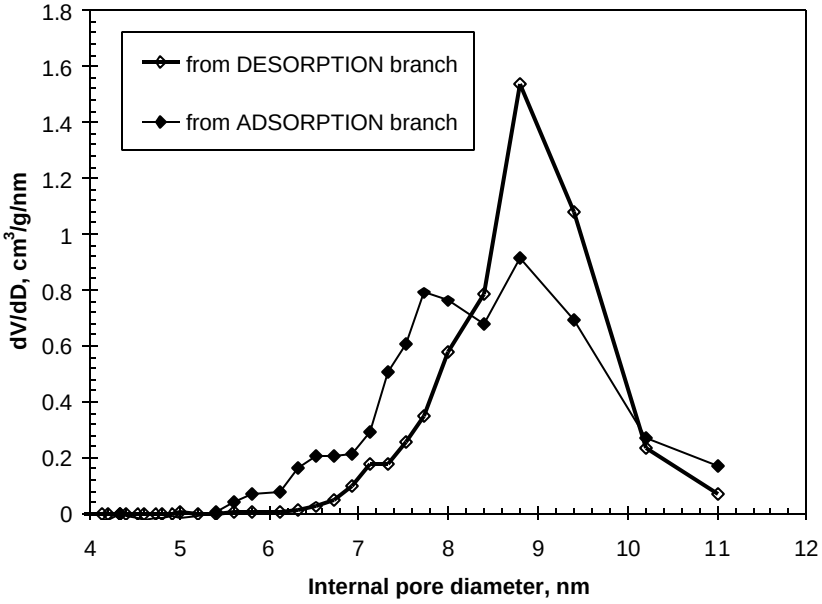

Figure 7. The pore size distribution of wide-pore material [4] (sample #4 in Table 1) calculated from adsorption and desorption branches of nitrogen isotherm by the NLDFT method.

Studies in Surf. Sci. & Catal., **2000**, v.129, p. 597-606.

Table 1
Pore structure parameters of enlarged MCM-41 materials [2-4]

Sample	a_0, nm	*Standard method*		*NLDFT method*					
		S_{BET}, m^2/g	V_p, cm^3/g	*Branch*	V_p^{DFT}, cm^3/g	S_p^{DFT}, m^2/g	D_p^{DFT} nm	σ_p^{DFT}, nm	d_{wall}, nm
#1	6.37	880	1.0	ads	0.97	790	5.1	0.34	1.3
				des	0.97	800	5.2	0.34	1.2
#2	6.80	880	1.07	ads	1.04	800	5.3	0.46	1.5
				des	1.04	805	5.4	0.49	1.4
#3	7.61	760	0.97	ads	0.96	690	5.8	0.54	1.8
				des	0.95	690	5.8	0.64	1.8
#4	n/a	1050	2.38	ads	2.2	1000	8.5	1.0	----
				des	2.2	1010	8.8	0.71	----

Samples #1, #2 and #3 are from Refs. [2, 3] (denoted 5.5 nm, 6.0 nm, and 6.5 nm therein).

Sample #4 is from Ref. [4] (sample E on Fig. 2 therein)

$a_0 = 2/\sqrt{3}\, d_{100}$ is a distance between pores calculated from X-ray diffraction data assuming hexagonal unit cell [2, 3].
S_{BET} was calculated using the molecular cross-sectional area of N_2, 0.162 nm^2/molecule.
V_p is the pore volume estimated from N_2 isotherms at P/P_o=0.6 (P/P_o=0.9 for sample #4) using the bulk liquid nitrogen density
V_p^{DFT} and S_p^{DFT} are the pore volume and the pore surface area, respectively, calculated by the NLDFT method.
D_p^{DFT} is the mean pore diameter calculated from the NLDFT pore size distribution
σ_p^{DFT} is the standard deviation calculated from the NLDFT pore size distribution
$d_{wall} = a_0 - D_p^{DFT}$ - the pore wall thickness assuming cylindrical pores

ACKNOWLEDGMENT

This work is supported by the EPA grant R825959-010, TRI/Princeton exploratory research program, and Quantachrome Corporation.

REFERENCES

1. C.T. Kresge, M.E. Leonowicz, W.J. Roth, J.C. Vartuli, J.S. Beck, Nature 359 (1992) 710.
2. A. Sayari, P. Liu, M. Kruk, and M. Jaroniec, Chem. Mater., 9 (1997) 2499.
3. M. Kruk, M. Jaroniec, A. Sayari, Langmuir, 13 (1997) 6267.
4. A. Sayari, M. Kruk, M. Jaroniec, I.L. Moudrakovski, Adv. Mater., 10 (1998) 1376.
5. D. Zhao, J. Feng, Q. Huo, N. Melosh, G.H. Fredrickson, B.F. Chmelka, G.D. Stucky, Science 279 (1998) 548.
6. D. Zhao, P. Yang, N. Melosh, J. Feng, B.F. Chmelka, G.D. Stucky, Adv. Mater. 10 (1998) 1380.
7. G.D. Stucky, Q. Huo, A. Firouzi, B.F. Chmelka, S. Schacht, I.G. Voigt-Martin, F. Schüth, Stud. Surf. Sci. Catal., 105A, (1997) 3.
8. L.H. Cohan, J. Amer. Chem. Soc. 60 (1938) 433.
9. B.V. Derjaguin, Acta Physicochim URSS 12 (1940) 181.
10. J.C.P. Broekhoff, J.H. de Boer, J. Catalysis 9 (1967) 8; ibid. 9 (1967) 15.
11. J.C.P. Broekhoff, J.H. de Boer, J. Catalysis 10 (1968b) 368; ibid. 10 (1968) 377.
12. D.H. Everett, in The Solid-Gas Interface, E.A. Flood (ed.), Marcel Decker, New York, vol. 2, (1967) p.1055
13. M.W. Cole, W.F. Saam, Phys. Rev. Lett. 32 (1974) 985.
14. S.J. Gregg and K.S.W. Sing, Adsorption, Surface Area and Porosity, Academic Press, London, 1982.
15. K. Morishige, M. Shikimi, J. Chem. Phys. B 108 (1998) 7821.
16. C.G. Sonwane, S.K. Bhatia, Chem. Eng. Sci. 53 (1998) 3143.
17. M.W. Maddox; J.P. Olivier, K.E. Gubbins, Langmuir 13 (1997) 1737.
18. A. de Keizer, Th. Michalski, and G.H. Findenegg, Pure & Appl. Chem., 10 (1991) 1495.
19. P. Tarazona, U. Marini Bettolo Marconi, and R. Evans, Mol. Phys. 60 (1987) 573.
20. P.I. Ravikovitch, S.C. Ó Domhnaill, A.V. Neimark, F. Schüth, K.K. Unger, Langmuir 11 (1995) 4765.
21. P.I. Ravikovitch, D. Wei, W.T. Chueh, G.L. Haller, A.V. Neimark, J. Phys. Chem. B 101 (1997) 3671.
22. P.I. Ravikovitch, G.L. Haller, A.V. Neimark, Adv. in Colloid Interface Sci. 76-77 (1998) 203.
23. A.V. Neimark, P.I. Ravikovitch, M. Grün, F. Schüth, and K.K. Unger, J. Coll. Interface Sci., 207 (1998) 159.
24. P.I. Ravikovitch, G.L. Haller, A.V. Neimark, Stud. Surf. Sci. Catal. 117 (1998) 77.
25. G.J. Tjatjopoulos, D.L. Feke, J.A. Mann Jr. J. Phys. Chem. 92 (1988) 4006.
26. J.H. de Boer, B.G. Linsen, Th.J. Osinga, J. Catalysis 4 (1965) 643.
27. M. Kruk, M. Jaroniec, A. Sayari, J. Phys. Chem. B 101 (1997) 583.
28. A.V. Neimark, P.I. Ravikovitch, A. Vishnyakov, submitted.
29. A.V. Neimark, Russian J. Phys. Chem. 60 (1986) 1045.
30. A.V. Neimark, Stud. Surf. Sci. Catal., 62 (1991) 67.